

## University of Nebraska - Lincoln DigitalCommons@University of Nebraska - Lincoln

Faculty Publications -- Chemistry Department

Published Research - Department of Chemistry

2019

# Electrocaloric effect in ferroelectric ceramics with point defects

Ming Wu

*Xi'an Jiaotong University*

Qingshan Zhu

*Xi'an Jiaotong University*

Jianting Li

*University of Science and Technology Beijing*

Dongsheng Song

*National University of Singapore*

Honghui Wu

*University of Nebraska - Lincoln*

*See next page for additional authors*

Follow this and additional works at: <https://digitalcommons.unl.edu/chemfacpub>

 Part of the [Analytical Chemistry Commons](#), [Medicinal-Pharmaceutical Chemistry Commons](#), and the [Other Chemistry Commons](#)

Wu, Ming; Zhu, Qingshan; Li, Jianting; Song, Dongsheng; Wu, Honghui; Guo, Mengyao; Gao, Jinghui; Bai, Yang; Feng, Yujun; Pennycook, Stephen J.; and Lou, Xiaojie, "Electrocaloric effect in ferroelectric ceramics with point defects" (2019). *Faculty Publications -- Chemistry Department*. 156.

<https://digitalcommons.unl.edu/chemfacpub/156>

This Article is brought to you for free and open access by the Published Research - Department of Chemistry at DigitalCommons@University of Nebraska - Lincoln. It has been accepted for inclusion in Faculty Publications -- Chemistry Department by an authorized administrator of DigitalCommons@University of Nebraska - Lincoln.

---

**Authors**

Ming Wu, Qingshan Zhu, Jianting Li, Dongsheng Song, Honghui Wu, Mengyao Guo, Jinghui Gao, Yang Bai, Yujun Feng, Stephen J. Pennycook, and Xiaojie Lou

# Electrocaloric effect in ferroelectric ceramics with point defects

Cite as: Appl. Phys. Lett. **114**, 142901 (2019); doi: [10.1063/1.5090183](https://doi.org/10.1063/1.5090183)

Submitted: 25 January 2019 · Accepted: 24 March 2019 ·

Published Online: 8 April 2019






View Online



Export Citation



CrossMark

Ming Wu,<sup>1,2</sup> Qingshan Zhu,<sup>3</sup> Jianting Li,<sup>4</sup> Dongsheng Song,<sup>2</sup> Honghui Wu,<sup>5</sup>  Mengyao Guo,<sup>1</sup> Jinghui Gao,<sup>1</sup> Yang Bai,<sup>4</sup>  Yujun Feng,<sup>3</sup> Stephen J. Pennycook,<sup>2</sup> and Xiaojie Lou<sup>1,a)</sup> 

## AFFILIATIONS

<sup>1</sup>Frontier Institute of Science and Technology, and State Key Laboratory for Mechanical Behavior of Materials, Xi'an Jiaotong University, Xi'an 710049, People's Republic of China

<sup>2</sup>Department of Materials Science and Engineering, National University of Singapore, 9 Engineering Drive 1, Singapore 117575

<sup>3</sup>Electronic Materials Research Laboratory, Key Laboratory of the Ministry of Education, Xi'an Jiaotong University, Xi'an 710049, People's Republic of China

<sup>4</sup>Key Laboratory of Environmental Fracture (Ministry of Education), University of Science and Technology Beijing, Beijing 100083, People's Republic of China

<sup>5</sup>Department of Chemistry, University of Nebraska, Lincoln, Nebraska 68588-0304, USA

<sup>a)</sup> Author to whom correspondence should be addressed: [xlou03@mail.xjtu.edu.cn](mailto:xlou03@mail.xjtu.edu.cn).

## ABSTRACT

The electrocaloric effect has drawn much attention due to its potential application in cooling devices. A negative electrocaloric effect is predicted to be induced in defect-doped ferroelectrics by computational results [A. Grünebohm and T. Nishimatsu, Phys. Rev. B **93**, 134101 (2016) and Ma *et al.*, Phys. Rev. B **94**, 094113 (2016)], but it need to be confirmed by experimental results. In this work, we prepared a 1 mol. % Mn-doped Pb(Zr<sub>0.2</sub>Ti<sub>0.8</sub>)O<sub>3</sub> ceramics (Pb((Zr<sub>0.2</sub>Ti<sub>0.8</sub>)<sub>0.99</sub>Mn<sub>0.01</sub>)O<sub>3</sub>), and the electrocaloric effect of the defect-containing ferroelectric ceramics has been investigated by both direct and indirect methods. The indirect method shows a similar negative electrocaloric effect signal as the computational results predicted, while the direct method gives a positive electrocaloric effect. The absence of the negative electrocaloric effect obtained by the direct method may originate from: (a) the unavailability and the improper prediction of the Maxwell relation, (b) an improper assumption of fixed defects in the computational models, and (c) the offset of heat loss due to the application of a large electric field. In addition, we find a giant positive electrocaloric effect of 0.55 K at room temperature in the aged ceramics where no phase transition takes place. We attribute this abnormal electrocaloric effect to the restoration force of the defect dipoles. Our results not only provide insights into the origin of the negative electrocaloric effect, but also offer opportunities for the design of electrocaloric materials.

Published under license by AIP Publishing. <https://doi.org/10.1063/1.5090183>

Electrocaloric materials have attracted much attention in recent decades due to their promising applications in solid-state cooling devices as well as the compatibility with integrated circuits.<sup>1–4</sup> The electrocaloric effect (ECE) describes the temperature change in the material when applying or withdrawing an external electric field, and it is of two types, that is, a positive ECE wherein applying the electric field induces a temperature increase and a negative ECE wherein applying the electric field induces a temperature drop.<sup>5–7</sup> However, different from the relatively simple positive ECE, the origin of negative ECE is still unclear (or under debate). More understanding about the origin of the negative ECE can help us to avoid the offset of the negative ECE on the positive ECE when designing electrocaloric materials/devices.<sup>8</sup> In addition, some researchers suggest that a combination of positive

and negative ECEs can enhance the overall temperature change, and thus increase the cooling efficiency.<sup>8,9</sup>

Experimentally, negative ECE can be indirectly estimated based on the Maxwell relation and also be directly measured by monitoring the change in the temperature or heat flow of the materials. PbZrO<sub>3</sub> and PbZrO<sub>3</sub> based antiferroelectrics are mainly reported to be negative ECE materials. The negative ECE in PbZrO<sub>3</sub> ceramics is identified by a direct measurement with a temperature change of  $-0.16$  K by using a bead thermistor.<sup>10</sup> Soon after, an enhanced negative ECE was indirectly predicted in La-doped PbZrO<sub>3</sub> thin films with a temperature change of  $-5$  K<sup>11</sup> and in Eu-doped PbZrO<sub>3</sub> thin films with a temperature change of  $-6.6$  K,<sup>12</sup> by using the Maxwell relation. Apart from antiferroelectrics, the negative ECE was also directly measured in

ferroelectrics with different ferroelectric phase transitions.<sup>9,13,14</sup> In addition, it is predicted that a negative ECE would exist in a ferroelectric with polar defect dipoles, as calculated by Monte-Carlo simulation and molecular dynamics simulation.<sup>15,16</sup> However, these theoretic predictions need to be further confirmed by experimental results.

In this work, we studied the ECE in ferroelectric ceramics containing defect dipoles. A typical tetragonal ferroelectric  $\text{Pb}(\text{Zr}_{0.2}\text{Ti}_{0.8})\text{O}_3$  (PZT) was chosen as the matrix and 1 mol. % Mn was doped into the B site of  $\text{Pb}(\text{Zr}_{0.2}\text{Ti}_{0.8})\text{O}_3$  to introduce defects, forming  $\text{Pb}(\text{Zr}_{0.2}\text{Ti}_{0.8})_{0.99}\text{Mn}_{0.01}\text{O}_3$ , henceforth denoted as PZTM. The distribution of the defects in PZTM ceramics was controlled in different stages, and the corresponding ECEs were measured by both a direct method based on modified differential scanning calorimetry (DSC) and an indirect method based on the Maxwell relation. It was found that the indirect method gives a negative ECE, while the direct method reports a positive ECE. In addition, in the aged PZTM ceramics, we report a large temperature change of 0.55 K with a composition far away from phase transition. Our results may offer an additional approach for choosing and designing electrocaloric materials.

The details about the materials preparation, characterization and indirect and direct methods of ECE measurement can be found in [supplementary material](#).

The effect of defect doping on the structure of PZTM ceramics is characterized on different scales, and the results are shown in [Fig. 1](#). In the X-ray diffraction (XRD) pattern, all peaks are found to be indexed, which indicates a pure perovskite structure without any second phase. The scanning electron microscopy image and energy dispersive X-ray spectroscopy mapping show an average grain size of about 20  $\mu\text{m}$  and a homogenous distribution of Mn in the PZTM ceramics, as seen in [Fig. S1](#) in [supplementary material](#). The bright field transmission electron microscopy image in [Fig. 1\(b\)](#) shows a typical stripe domain with a size of hundreds of nanometers, which is widely observed in tetragonal phased ferroelectric ceramics.<sup>17</sup> To check the influence of Mn doping on the local structure of the PZTM ceramic, one of the

[110] oriented crystals was chosen and an atomic resolution high angle annular dark field (HAADF) image from a scanning transmission electron microscope (STEM) was captured, as shown in [Fig. 1\(c\)](#). In such a Z-Contrast image, the much brighter contrast represents the Pb positions, while the much fainter features in-between represent Zr/Ti atom columns.<sup>18</sup> Clearly, doping 1 mol. % Mn neither affects the microstructure nor destroys the local lattice of the PZTM ceramics.

The ferroelectric-paraelectric phase transition of PZTM ceramics was confirmed by the abnormal peak at 457 °C (that is, the Curie point) in the temperature dependence of dielectric constant. It is because of such high Curie temperature that we can observe the pinched hysteresis loops at room temperature in the as-prepared defect-doped PZTM ceramics, as shown in [Fig. 2\(b\)](#). The substitution of  $\text{Ti}^{4+}/\text{Zr}^{4+}$  by  $\text{Mn}^{2+}$  induces oxygen vacancies for charge neutrality. The negatively charged  $\text{Mn}^{2+}$  defects and the positively charged oxygen vacancies tend to form defect dipoles, and the configuration of defect dipoles follows the domain pattern of the ferroelectric polarization [as shown in [Fig. 3\(a\)](#)] to lower the total energy of the system.<sup>19</sup> This process is called the aging effect.<sup>19</sup> In this case, due to the high Curie temperature of the PZTM ceramics, a very fast aging process appears during the furnace cooling process after sintering the ceramics. Similar fast aging phenomena can also be seen in (K, Na)NbO<sub>3</sub>-based ceramics.<sup>20,21</sup>

The response of defect dipoles to the electric field is much slower than the switching of polarization by the electric field.<sup>22,23</sup> To detect the effect of defect dipoles on the switching of polarization, the frequency dependence of hysteresis loops is measured, and the results are shown in [Fig. 2\(c\)](#). The polarization switching is slightly enhanced when the frequency decreases from 50 Hz to 10 Hz. With a further decrease of the frequency to 1 Hz, a significant increase in polarization is observed, which indicates the reduced pinning effect of the defects on the polarization switching. To further observe the switching of defect dipoles at the low-frequency electric field, the hysteresis loops are tested at elevated temperatures, that is, 90 °C, to enhance the diffusion of defects. The evolution of hysteresis loops under the application

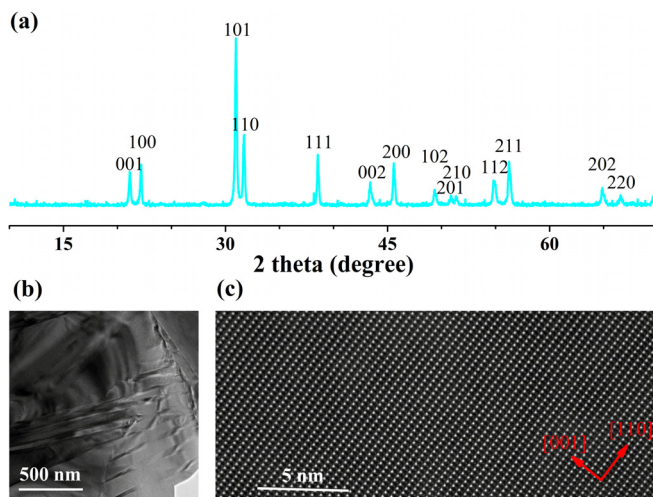


**FIG. 1.** Macro-, micro-, and local-structures of the PZTM ceramics characterized by (a) XRD, (b) bright field transmission electron microscopy and (c) HAADF STEM, viewed along the [110] zone axis.

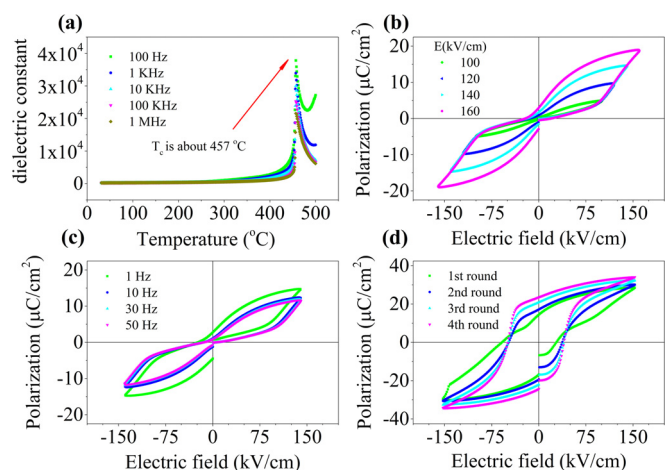


**FIG. 2.** (a) Temperature dependence of dielectric constant. Hysteresis loops measured at (b) 10 Hz with different electric fields and (c) 140 kV/cm at different frequencies. (d) Hysteresis loop evolution under a 1 Hz electric field at 90 °C.

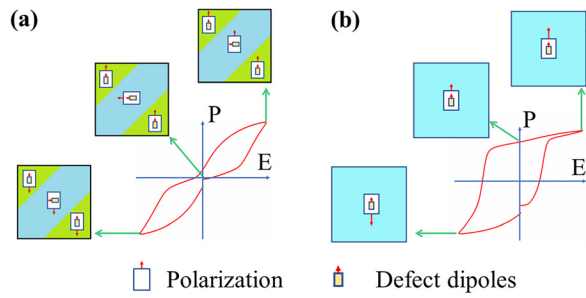


**FIG. 3.** Schematic of the effect of defect distribution on polarization switching at room temperature when the defects are (a) in the aging state and (b) after poling by applying a unipolar positive field. The filled squares represent the defect dipoles in a multi-domain configuration in the aging state and in a single domain configuration after poling. The large unfilled and small filled rectangles with red arrows represent the direction of ferroelectric polarization and defect dipoles, respectively. The length of the arrow represents the strength of the polarization.

of the electric field at a frequency of 1 Hz is shown in Fig. 2(d). From the first to fourth round application of the electric field, the pinched double loop changes into a single loop.

Thus, the ECEs of the PZTM ceramics are studied with the defects distributed in two states, that is, in an aging state and after poling. The distribution of the defects as well as its effect on the switching of the ferroelectric polarization is schematically shown in Fig. 3.

The ECE of the PZTM ceramics is firstly investigated by both the indirect method and the direct method when the defect dipoles are in the aging state. The configuration of defect dipoles follows the ferroelectric domain structure in the aging state and exhibits zero remanent polarization without the application of the electric field, as shown in Fig. 3(a). When applying the electric field, the defect dipoles remain unswitchable, while the polarization switches. Figure 4(a) shows the polarization-temperature (P-T) curves, where a gradually increased polarization with elevated temperatures is observed. Correspondingly,

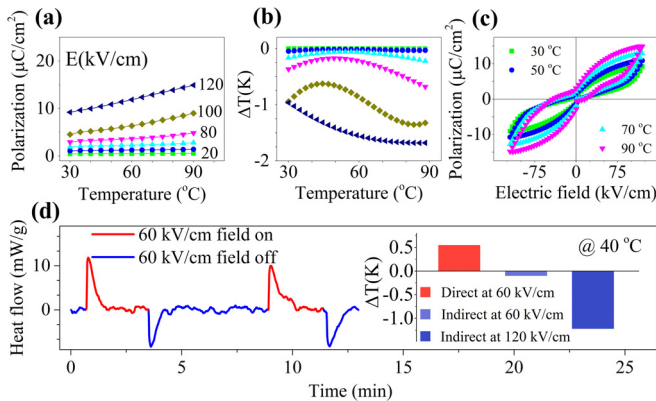


**FIG. 4.** ECE of the PZTM ceramic with defects in the aging state. (a) P-T curves. (b) Temperature change estimated by the indirect method based on Maxwell's relation. (c) Representative hysteresis loops under application of an electric field of 120 kV/cm. (d) Directly measured heat flow (that is, the DSC signal curve) on the application and removal of the electric field of 60 kV/cm at 40 °C. The inset shows the comparison of the temperature change measured by both the direct method and the indirect method.

the temperature change estimated by Maxwell's relation shows a negative ECE in the whole temperature range at every applied electric field. In contrast, as shown in Fig. 4(d), the DSC heat flow shows an exothermic peak with the applied electric field of 60 kV and an endothermic peak on removal of the electric field, indicating a positive ECE.<sup>9</sup> It is found that the exothermic peaks are slightly bigger than the endothermic peaks. As suggested by Weyland *et al.*,<sup>24</sup> this phenomenon may be induced by hysteresis loss. The endothermic peaks are used to calculate the ECE as it is most relevant for most applications. As compared in the inset of Fig. 4(d), the direct method measures a positive ECE of 0.55 K under the electric field of 60 kV/cm at 40 °C, while the indirect method predicts a negative ECE of -0.1 K under the same conditions, and a further enhanced negative ECE up to -1.22 K is predicted by the indirect method when the electric field is increased to 120 kV/cm.

The PZTM ceramics are also poled (at 90 °C for 10 min under an electric field of 90 kV/cm) to align the defect dipoles. The hysteresis loops and the distribution of the defects in the PZTM ceramics are schematically shown in Fig. 3(b). The orientation of defect dipoles follows the poling direction, and also, the defect dipoles cannot be rotated by the high frequency electric field. The heat flow of the PZTM ceramics during the poling process is shown in Figs. 5(d)-5(i). The elevated baseline with the application of the electric field is due to the Joule heat induced by the movement/redistribution of the charged defects. Figure 5(c) shows the hysteresis loops of the poled PZTM ceramic at 30 °C, 50 °C, 70 °C, and 90 °C under electric fields of 80 kV/cm and 120 kV/cm. From the hysteresis loops at 30 °C, the

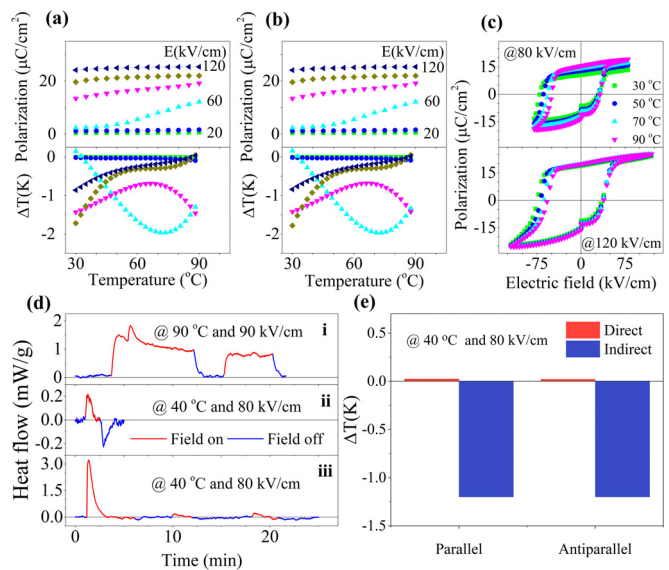


**FIG. 5.** ECE of the PZTM ceramics with defects in the poled state. P-T curves as well as the estimated temperature change from the (a) 1st and (b) 3rd quadrants of the hysteresis loops. (c) Representative hysteresis loops at 80 kV/cm and 120 kV/cm at various temperatures. DSC heat flow of the PZTM ceramics with application and removal of electric fields of 90 kV/cm at 90 °C (d-i) and at 80 kV/cm and 40 °C with the electric field parallel (d-ii) and antiparallel (d-iii) to the defect dipoles, respectively. (e) The comparison of the ECE determined by direct and indirect methods when the applied electric field is parallel or antiparallel to the defect dipoles.

room temperature internal electric field ( $E_{in}$ ) induced by the aligned defect dipoles can be estimated as  $-18.5$  kV/cm by the left coercive field ( $E_{lc}$ ) of  $-73$  kV/cm and the right coercive field ( $E_{rc}$ ) of  $36$  kV/cm [ $E_{in} = (E_{lc} + E_{rc})/2$ ]. The polarization extracted from the 1st (3rd) quadrant represents the polarization induced by the electric field parallel (antiparallel) to the internal electric field. The absolute values of polarization (that is,  $|P|$ ) in the 3rd quadrant are used for the indirect calculation. The P-T curves extracted from the 1st and 3rd quadrants of the hysteresis loop are shown in Figs. 5(a) and 5(b), and the corresponding ECE estimated by the indirect method are also plotted. With both parallel and antiparallel defect dipoles, the indirect method predicts a negative ECE, and the difference is negligible. The direct measurements of heat flow with the applied electric field parallel and antiparallel to the defect dipoles are shown in Figs. 5(d-ii) and 5(d-iii), respectively. A very small exothermic and an endothermic peak can be observed when the electric field of  $80$  kV/cm (parallel to the defect dipole's direction) is applied or removed, indicating a positive ECE signal, as shown in Fig. 5(d-ii). When the applied electric field is reversed, (that is, antiparallel to the defect dipoles), a relatively bigger exothermic peak is observed first, followed by a negligible endothermic peak [see Figs. 5(d-iii)]. The abnormal exothermic peak may be induced by hysteresis loss during polarization switching. With further applying or removing the electric field, the polarization shows the same direction as the applied field. Therefore, the abnormal exothermic peak disappears and the change of heat flow becomes very weak, but, showing a positive ECE. The comparison of ECEs estimated by direct and indirect methods is shown in Fig. 5(e). The direct method estimates a positive ECE of  $0.025$  K and  $0.022$  K in parallel defect dipoles and antiparallel defect dipoles, respectively. But the indirect method predicts a negative ECE of about  $-1.2$  K in both cases.

Whether in the aging or the poled state, the direct method estimates a positive ECE, while the indirect method predicts a negative ECE. The results from the direct method are much more reliable since it is calculated from the direct measurement of heat flow, and thus the indirect method predicts a false negative ECE in the defect-doped PZT ceramics. A false negative ECE may be induced by the unavailability of Maxwell's relation. The application of Maxwell's relation requires fully saturated polarization under application of the electric field,<sup>25</sup> while in this case the pinning effect of defects results in unsaturated polarization switching. Similar discrepancy has also been reported in (Bi, Na)TiO<sub>3</sub> based ceramics.<sup>26</sup> The defects induced by Mn doping pin the ferroelectric domain, resulting in nearly non-switching of the ferroelectric domain under a low electric field, as represented by the P-T curves below  $80$  kV/cm in the aging state [Fig. 4(a)]. As the electric field is increased further (above  $80$  kV/cm in the aging state), the domain starts to switch and the pinning of the defects becomes loose at elevated temperatures, resulting in increased polarization. The switching is still unsaturated until the maximum electric field of  $120$  kV/cm is applied, due to the large resistance of domain switching in the aging state [the evaluation of P-T curves is shown in Fig. 4(a)]. The polarization starts to increase with increasing temperature under an electric field of  $60$  kV/cm [Figs. 5(a) and 5(b)] and nearly saturates at an electric field of  $120$  kV/cm, as identified by the hysteresis loops shown in Fig. 5(c). It is believed that with a further increase of the electric field, e.g.,  $140$  kV/cm, the P-T curves would show a decreased tendency, giving rise to a positive ECE. Unfortunately, the PZTM ceramics break down at such a high electric field and temperature. In addition, since

the defects are more sensitive to the low-frequency electric field, the possible re-distribution/diffusion of the defects under a direct-current electric field during direct measurements may also lead to the discrepancy of the ECE as estimated by the direct and indirect methods.

Previously, computational results predicted a negative ECE in defect-doped BaTiO<sub>3</sub> when the applied electric field is antiparallel to the defect dipoles.<sup>15,16</sup> However, only a positive ECE is observed in our PZTM ceramics. This discrepancy may result from the following aspects. Firstly, in the computational model, the defect dipoles are assumed as fixed, and become neither switchable nor movable under the application of the electric field. However, in the real case, the switching and movement of defect dipoles are inevitable. Application of the reversed electric field may also induce dissociation of the antiparallel defect dipoles.<sup>27</sup> Besides, the application of a large electric field would induce significant heat losses, which would offset the negative ECE, as discussed by Ma *et al.*<sup>28</sup> In fact, the inverted ECE has already been observed in Fe-doped PZT ceramics with the application of a smaller electric field.<sup>24</sup> And, this negative ECE changed into positive with a further increase of the electric field. We also tried to measure the ECE under a smaller electric field by using the direct method, but unfortunately the signal is too noisy to distinguish from the baseline.

In addition, it is surprising to obtain a giant temperature change of  $0.55$  K in the aged PZTM ceramic by using a direct method under an electric field of  $60$  kV/cm. Such a giant value is commonly observed in the temperature range that includes phase transitions<sup>29-31</sup> or multi-phase coexistence,<sup>32-34</sup> while no phase transition is identified in the temperature dependence of dielectric constant [Fig. 2(a)]. It is known that when the electric field is applied for the first time, the polarization is switched from zero, resulting in a giant exothermic peak. However, the polarization cannot switch back to zero on removal of the electric field, which induces a much smaller endothermic peak. However, the defect dipoles in the PZTM ceramics impose a restoration force, ensuring zero net remanent polarization on removal of the electric field, as schematically shown in Fig. 3(a). Similarly, the restoration force of the aged defect dipoles has also been used to enhance the strain of the Fe-doped BaTiO<sub>3</sub> single crystal.<sup>19</sup> Combined with composition designing and phase transition controlling, the restoration force induced by the defect doping can further enhance the ECE of the materials, and thus promote the application of ECE materials.

In conclusion, the ECE of Mn-doped PZT ceramics is estimated by both direct and indirect methods. The direct method reports a positive ECE, while the indirect method predicts a false negative ECE. It is believed that the negative ECE is an artifact induced by the unavailability of the Maxwell relation. Remarkably, a giant temperature change of  $0.55$  K was measured in the aged PZTM ceramics where no phase transition takes place. We attribute this enhancement to a restoration force of the defect dipoles. Our results show opportunities to regulate and enhance the ECE of ferroelectrics without changing the phase structure or the phase transition temperature, indicating a promising application in designing ECE materials and devices.

See [supplementary material](#) for the SEM image, EDX results and the experiment details.

This work was supported by the National Science Foundation of China (NSFC No. 51772238), the CSS project (Grant No. YK2015-0602006),

the Fundamental Research Funds for the Central Universities, and the World-Class Universities (Disciplines) and the Characteristic Development Guidance Funds for the Central Universities. Wu Ming would like to thank the Chinese Scholarship Council (Grant No. 201706280322) for support.

## REFERENCES

- <sup>1</sup>S. Lu, B. Rožič, Q. Zhang, Z. Kutnjak, X. Li, E. Furman, L. J. Gorný, M. Lin, B. Malič, and M. Kosec, *Appl. Phys. Lett.* **97**, 162904 (2010).
- <sup>2</sup>A. Mischenko, Q. Zhang, J. Scott, R. Whatmore, and N. Mathur, *Science* **311**, 1270 (2006).
- <sup>3</sup>A. Mischenko, Q. Zhang, R. W. Whatmore, J. Scott, and N. Mathur, *Appl. Phys. Lett.* **89**, 242912 (2006).
- <sup>4</sup>B. Neese, B. Chu, S.-G. Lu, Y. Wang, E. Furman, and Q. Zhang, *Science* **321**, 821 (2008).
- <sup>5</sup>X.-D. Jian, B. Lu, D.-D. Li, Y.-B. Yao, T. Tao, B. Liang, J.-H. Guo, Y.-J. Zeng, J.-L. Chen, and S.-G. Lu, *ACS Appl. Mater. Interfaces* **10**, 4801 (2018).
- <sup>6</sup>B. Lu, Y. Yao, X. Jian, T. Tao, B. Liang, Q. Zhang, and S.-G. Lu, *J. Eur. Ceram. Soc.* **39**, 1093 (2019).
- <sup>7</sup>B. Lu, P. Li, Z. Tang, Y. Yao, X. Gao, W. Kleemann, and S.-G. Lu, *Sci. Rep.* **7**, 45335 (2017).
- <sup>8</sup>A. Grünebohm, Y. B. Ma, M. Marathe, B. X. Xu, K. Albe, C. Kalcher, K. C. Meyer, V. V. Shvartsman, D. C. Lupascu, and C. Ederer, *Energy Technol.* **6**, 1491 (2018).
- <sup>9</sup>J. Li, S. Qin, Y. Bai, J. Li, and L. Qiao, *Appl. Phys. Lett.* **111**, 093901 (2017).
- <sup>10</sup>R. Pirc, B. Rožič, J. Koruza, B. Malič, and Z. Kutnjak, *EPL-Europhys. Lett.* **107**, 17002 (2014).
- <sup>11</sup>W. Geng, Y. Liu, X. Meng, L. Bellaiche, J. F. Scott, B. Dkhil, and A. Jiang, *Adv. Mater.* **27**, 3165 (2015).
- <sup>12</sup>M. Ye, T. Li, Q. Sun, Z. Liu, B. Peng, C. Huang, P. Lin, S. Ke, X. Zeng, and X. Peng, *J. Mater. Chem. C* **4**, 3375 (2016).
- <sup>13</sup>J. Peräntie, J. Hagberg, A. Uusimäki, and H. Jantunen, *Phys. Rev. B* **82**, 134119 (2010).
- <sup>14</sup>F. L. Goupil, A. Berenov, A.-K. Axelsson, M. Valant, and N. M. Alford, *J. Appl. Phys.* **111**, 124109 (2012).
- <sup>15</sup>A. Grünebohm and T. Nishimatsu, *Phys. Rev. B* **93**, 134101 (2016).
- <sup>16</sup>Y.-B. Ma, A. Grünebohm, K.-C. Meyer, K. Albe, and B.-X. Xu, *Phys. Rev. B* **94**, 094113 (2016).
- <sup>17</sup>D. I. Woodward, J. Knudsen, and I. M. Reaney, *Phys. Rev. B* **72**, 104110 (2005).
- <sup>18</sup>S. J. Pennycook, C. Li, M. Li, C. Tang, E. Okunishi, M. Varela, Y.-M. Kim, and J. H. Jang, *J. Anal. Sci. Technol.* **9**, 11 (2018).
- <sup>19</sup>X. Ren, *Nat. Mater.* **3**, 91 (2004).
- <sup>20</sup>D. Lin, K. W. Kwok, and H. Wong Lai-wa Chan, *J. Am. Ceram. Soc.* **92**, 1362 (2009).
- <sup>21</sup>J. Hao, Z. Xu, R. Chu, W. Li, J. Du, P. Fu, and G. Li, *J. Am. Ceram. Soc.* **99**, 402 (2016).
- <sup>22</sup>J. F. Scott, *Ferroelectric Memories* (Springer Science & Business Media, 2013), Vol. 3.
- <sup>23</sup>S.-J. Lee, K.-Y. Kang, and S.-K. Han, *Appl. Phys. Lett.* **75**, 1784 (1999).
- <sup>24</sup>F. Weyland, A. Bradeško, Y. B. Ma, J. Koruza, B. X. Xu, K. Albe, T. Rojac, and N. Novak, *Energy Technol.* **6**, 1519 (2018).
- <sup>25</sup>F. Le Goupil, J. Bennett, A.-K. Axelsson, M. Valant, A. Berenov, A. J. Bell, T. P. Comyn, and N. M. Alford, *Appl. Phys. Lett.* **107**, 172903 (2015).
- <sup>26</sup>E. Birks, M. Duce, J. Peräntie, J. Hagberg, and A. Sternberg, *J. Appl. Phys.* **121**, 224102 (2017).
- <sup>27</sup>P. Erhart, P. Träskelin, and K. Albe, *Phys. Rev. B* **88**, 024107 (2013).
- <sup>28</sup>Y.-B. Ma, B.-X. Xu, K. Albe, and A. Grünebohm, *Phys. Rev. Appl.* **10**, 024048 (2018).
- <sup>29</sup>X. Wang, J. Wu, B. Dkhil, B. Xu, X. Wang, G. Dong, G. Yang, and X. Lou, *Appl. Phys. Lett.* **110**, 063904 (2017).
- <sup>30</sup>X. Wang, F. Tian, C. Zhao, J. Wu, Y. Liu, B. Dkhil, M. Zhang, Z. Gao, and X. Lou, *Appl. Phys. Lett.* **107**, 252905 (2015).
- <sup>31</sup>H. Wu and R. Cohen, *J. Phys. Condens. Matter* **29**, 485704 (2017).
- <sup>32</sup>J. Li, D. Zhang, S. Qin, T. Li, M. Wu, D. Wang, Y. Bai, and X. Lou, *Acta Mater.* **115**, 58 (2016).
- <sup>33</sup>Z. Luo, D. Zhang, Y. Liu, D. Zhou, Y. Yao, C. Liu, B. Dkhil, X. Ren, and X. Lou, *Appl. Phys. Lett.* **105**, 102904 (2014).
- <sup>34</sup>H. Wu and R. Cohen, *Phys. Rev. B* **96**, 054116 (2017).